THE UNIVERSITY OF

WARWICK

Original citation:
Khadidos, Alaa, Sanchez Silva, Victor and Li, Chang-Tsun (2014) Active contours with weighted external forces for medical image segmentation. In: The 18th Annual Conference in Medical Image Understanding and Analysis (MIUA2014), UK, London, 9-11 Jul 2014. Published in: Proceedings of The 18th Annual Conference in Medical Image Understanding and Analysis (MIUA2014)
Permanent WRAP url:
http://wrap.warwick.ac.uk/65174

A note on versions:
The version presented here is a working paper or pre-print that may be later published elsewhere. If a published version is known of, the above WRAP url will contain details on finding it.

For more information, please contact the WRAP Team at: publicatons@warwick.ac.uk

warwickpublicationswrap

highlight your research

http://wrap.warwick.ac.uk/

Active Contours with Weighted External Forces for Medical Image Segmentation

Alaa Khadidos[1][2]
A.Khadidos@warwick.ac.uk

Victor Sanchez[1]
vsanchez@dcs.warwick.ac.uk

Chang-Tsun Li[1]
C-T.Li@warwick.ac.uk

[1] University of Warwick
Department of Computer Science,
Coventry, UK

[2] King Abdulaziz University
Faculty of Computing and Information
Technology, Jeddah, Saudi Arabia

Abstract

Parametric active contours have been widely used for image segmentation. However, high noise levels and weak edges are the most acute issues that hinder their performance, particularly in medical images. In order to overcome these issues, we propose an external force that weights the gradient vector flow (GVF) field and balloon forces according to local image features. We also propose a mechanism to automatically terminate the contour's deformation. Evaluation results on real MRI and CT slices show that the proposed approach attains higher segmentation accuracy than snakes using traditional external forces, while allowing initialization using a limited number of selected points.

1   Introduction

Parametric active contours, or snakes, model the movement of a dynamic curve towards an object's boundary under the influence of internal and external forces [5, 9]. Parametric snakes produce closed and smooth object boundaries while allowing the separation of objects in contact by prohibiting contour fusions. The latter is an important advantage over non-parametric approaches, such as the level-set approach [16].

Despite the outstanding results of parametric snakes for image segmentation, their accuracy is relatively low when the amount of image clutter and noise is high [15]. In such cases, the use of various external forces that help the snake to conform to the desired boundary is an appropriate solution. For example, Cohen [2] propose *balloon* forces to guide the snake to the object's boundary in a similar way a balloon inflates or deflates. Xu *et al*. [12] propose the gradient vector flow (GVF) field as an external force to help the snake to conform to concave boundaries. Other proposals include using vector field convolution (VFC) as an external force, which is calculated by convolving the image edge map with a user-defined vector field kernel [7]; integrating the GVF field with prior directional information manually provided [15]; convolving the image with a sigmoid function before computing the GVF field [13]; adaptively computing the GVF field according to the characteristics of an image region [11];and computing a mean shift based GVF (MSGVF) to balance internal and external forces and drive the curve towards the desired boundary [14].

Although balloon forces may help guide the snake to the desired boundary over noise areas, the strength of the force must be appropriately set in order for the snake to detect weak edges and avoid snake leakages. GVF-based methods, and many of its variants, are proposed in order to address shortcomings of the balloon force; these external forces, however, may still require that the initial snake be initialized close to the desired boundary to obtain accurate segmentation results, particularly in noise images [1]. This inevitably involves manually

selecting several initial points or snake elements. Moreover, regardless of the external force used, the appropriate number of iterations to accurately conform the desired boundary must be carefully selected in an empirical manner.

In this work, we use an external force that combines the advantages of GVF and balloon forces, especially for cases when the snake is initialized far from the desired boundary in a noisy area and with a very limited number of snake elements [6]. Specifically, balloon forces are used to guide the snake to the object's boundary even in the presence of image clutter and noise; while GVF forces are used to improve segmentation accuracy even around weak edges. We control the effect of these two forces by a weighting function based on local image features. Also in this work, we propose a mechanism to terminate the snake's deformation process without having to manually indicate the number of iterations. The proposed approach minimizes snake leakages and considerably reduces the number of initial snake elements, making it suitable for medical image segmentation with little manual intervention.

2 Proposed External Force

A snake is a curve $C(s) = [x(s), y(s)]$, with $s \in [0, 1]$ at position (x, y), that evolves to an object's boundary by minimizing the energy functional $E_S = \int_0^1 [E_{int}(C(s)) + E_{ext}(C(s))]ds$, where $E_{int}(C(s)) = \frac{1}{2}(\alpha|C'(s)|^2 + \beta|C''(s)|^2)$ is the internal energy with α and β controlling the smoothness of C, and $E_{ext}(C(s))$ is the external energy, which attracts C towards the object's boundary. E_S can be minimized by evolving the snake dynamically as a function of parameter s and artificial time t; namely, $C(s, t) = \left[\alpha C''(s, t) - \beta C''''(s, t) \right] - \nabla E_{ext}$, where the first term and the second term are called the internal force, $F_{internal}$, and the external force, $F_{external}$, respectively.

Our external force is a weighted combination of balloon and GVF forces and aims at exploiting the advantages of each of these two forces. Balloon forces are represented as $F_{balloon} = n(s)$, where $n(s)$ is a unit vector normal to the snake at snake element C_n. GVF forces are derived from the diffusion of the gradient vectors of the image edge map $f(x, y)$, and are given as $F_{GVF} = v(x, y)$, where $v(x, y) = [u(x, y), v(x, y)]$ denotes the GVF field [12]. The proposed external force is then defined as $F_{external} = (F_{Balloon} * (1 - \Omega)) + (F_{GVF} * \Omega)$, where $\Omega \in [0, 1]$ is a weighting factor given by:

$$\Omega = \bar{h}^{(1 - (\bar{AD} - \varepsilon))} \tag{1}$$

where $\bar{h} \in [0, 1]$ denotes the average intensity value of $f(x, y)$ over a semi-circular region S of radius r centered at each snake element, and $\bar{AD} \in [0, 1]$ is the average angular difference between the direction of $F_{Balloon}$ and the direction of the GVF field over a cone-shaped region T centered at each snake element. $\bar{AD} = 0$ represents 0 rad, while $\bar{AD} = 1$ represents π rad. Constant $\varepsilon = 0.001$ prevents power by zero when $\bar{AD} = 1$. For each snake element at position (x, y), $\bar{h}$ and $\bar{AD}$ are calculated as follows:

$$\bar{h}(x, y) = \frac{1}{N} \sum_{(i,j) \in S} h(i, j); \quad \bar{AD}(x, y) = \frac{1}{M * \pi} \sum_{(i,j) \in T} \theta(i, j) \tag{2}$$

where N is the number of pixels located in region S, h is the edge intensity at position (i, j), M is the number of GVF field vectors in region T, and θ is the minimum angle between the GVF field vector at position (i, j) and $F_{Balloon}$ for snake element C_n at position (x, y), as illustrated in Fig. 1. Note that $T(x, y, sl, \varphi)$ is a cone-shaped region with its vertex in (x, y), which allows analyzing the region located far from snake element C_n and thus provides a better insight of the direction of the GVF field than the region close to C_n.
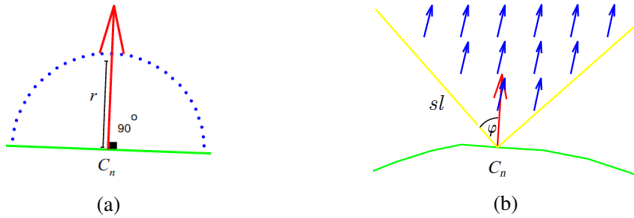
Figure 1: (a) Region S and (b) T for snake element C_n. The snake, the direction of $F_{Balloon}$, and the GVF field vectors are represented in green, red and blue, respectively.

The weighting function in Eq. (1) assigns different priorities to $F_{balloon}$ and F_{GVF} according to two local image features: the average edge intensity ($\bar{h}$) and the average GVF field direction ($\bar{AD}$). This weighting process helps to achieve the following:

1. Guide the snake to the boundary in smooth areas even if its normal direction of growth is opposite to F_{GVF}. This allows initialization far from the boundary with a limited number of snake elements. Fig. 2(a-b) illustrate this, where Ω approaches 0.
2. Minimize snake leakages around weak edges by averaging the edge intensity and the GVF field direction. Fig. 2(c) illustrates this, where Ω slowly approaches 1.
3. Conform to the desired boundary by assigning a higher weight to F_{GVF} when edges are encountered. This is illustrated in Fig. 2(d), where Ω approaches 1.
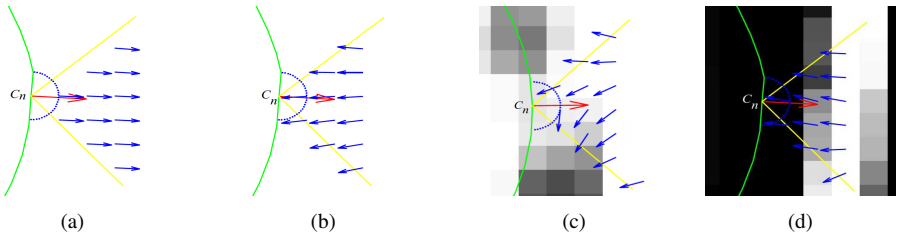

Figure 2: GVF field direction in region T (a) towards and (b) against the snake's growth ($\Omega \rightarrow 0$); and around (c) weak and (d) strong edges (non-white pixels represent strong edges).

In classical snakes, the deformation process is usually performed over a fixed number of iterations, over which it is expected to achieve convergence, i.e., external forces become zero. For images with strong edges, this number of iterations may be easily determined empirically. However, for images with weak edges, this number should be carefully selected to prevent leakages [8]. Here, we propose a mechanism to terminate the deformation process based on the percentage of snake elements labeled as *off*. A snake element is said to be *off* if no external force is acting on it. This usually occurs when the element encounters a strong edge, i.e., F_{GVF} is the main acting external force ($\Omega > 0.5$) and the overall strength of the GVF field around the element is close to zero. To this end, if $\Omega > 0.5$, we compute Ω_b in the same manner as Ω in Eq. (1), but using regions S_b and T_b, as illustrated in Fig. 3. We then label a snake element as *off* and set its forces to zero if $(\Omega_b)^2 > \Omega > 0.5$. This condition allows determining if the overall strength of the GVF field around the element is close to zero, i.e., the GVF field has opposite average directions in regions T and T_b. We use the squared value of Ω_b to prevent the element from *moving* past the edge. If the percentage of *off* snake elements is equal to or greater than Q, the whole deformation process is terminated.

3   Experimental Results

The performance of the proposed approach over several regions of real MRI and CT slices is compared to that of snakes using three different external forces: a) F_{GVF} exclusively [12], b) $F_{balloon}$ and image gradient (BGrad) forces [2], and c) F_{GVF} or $F_{balloon}$ (BGVFT)
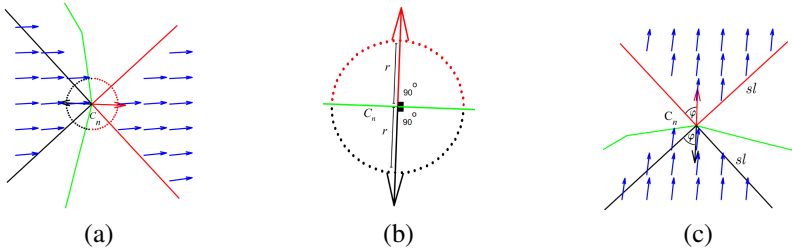
Figure 3: (a) Regions T and S (in red) used to compute Ω, and regions T_b and S_b (in black) used to compute Ω_b. (b) Dimension of regions S and S_b and of (c) regions T and T_b.

Table 1: Detection accuracy of snakes using various external forces.

Exp.	GVF		BGrad		BGVFT		Proposed approach		No. iterations
	DSC	JC	DSC	JC	DSC	JC	DSC	JC	
1	0.8716	0.7724	0.8795	0.7848	0.9341	0.8763	**0.9413**	**0.8902**	43
2	0.9329	0.8742	0.8969	0.8130	0.9368	0.8812	**0.9517**	**0.9079**	45
3	0.9041	0.8249	0.8840	0.7921	0.9374	0.8822	**0.9537**	**0.9115**	44
4	0.9311	0.8710	0.8676	0.7662	0.9365	0.8806	**0.9559**	**0.9154**	38
5	0.9345	0.8770	0.8493	0.7380	0.9612	0.952	**0.9631**	**0.9288**	43
6	0.1445	0.0779	0.8017	0.6691	0.9517	0.9078	**0.9643**	**0.9311**	96
7	0.0044	0.0022	0.6877	0.5240	0.8996	0.8174	**0.9709**	**0.9453**	171
8	0.9381	0.8834	0.9045	0.8256	**0.9568**	**0.9171**	0.9433	0.8926	45
9	0.9043	0.8253	0.8263	0.7040	**0.9393**	**0.8855**	0.9310	0.8709	26
10	0.9258	0.8619	0.6844	0.5202	0.9231	0.8541	**0.9426**	**0.8915**	60

according to a threshold i.e., if $\bar{h} > 0.05$ the acting external force is then set to F_{GVF}. All images are preprocessed using histogram equalization to enhance edges. The edge map $f(x, y)$ is computed using the wavelet coefficients obtained after applying the stationary wavelet transform (SWT) using the Haar filter with $L = 3$ levels of decomposition, as explained in [10]. We use all parameter values suggested in [12] to compute the GVF field and to control the snake's smoothness. We use a radius $r = 1$ pixels for regions S and S_b, an angle $\varphi = 45^o$ and $sl = 5$ pixels for regions T and T_b. These values provide the best trade-off between capturing enough local image features and computational complexity. All snakes are initialized inside the desired region by manually selecting a single position that is used as the center of an initial circular curve of p pixels in radius. The whole deformation process is terminated if more than $Q = 90\%$ of the snake elements are labeled as *off*.

The detection accuracy of the evaluated methods is measured by the Dice similarity (DSC) [3] and Jaccard coefficients (JC) [4] using manually annotated ground truth. DSC and JC values are within the range $[0, 1]$, where 1 indicates identical overlap and 0 indicates no overlap between the regions inside the detected boundaries. Table 1 tabulates the DSC and JC values for different regions of MRI and CT slices. Experiments 1-3 represent three different regions of an MRI slice of a spinal cord, 4 and 5 represent two regions of an MRI slice of a pelvis, 6 and 7 represent two regions of an MRI slice of a knee, 8 represents one region of a CT slice of a skull, and 9 and 10 represent two regions of a CT slice of a spinal cord. In all experiments, the number of iterations is equal for all evaluated methods and is set to the number of iterations required by our termination mechanism. Results in Table 1 show that our approach achieves the highest accuracy for the majority of experiments. Note that for experiments 8-9, the BGVFT snake achieves higher DCS and JC values than our approach for the same number of iterations. In these cases, the BGVFT snake effectively switches between GVF and balloon forces based on the selected threshold. However, the BGVFT snake, similarly to the GVF and BGrad snakes, requires manual selection of the

(a) 5 iterations   (b) 20 iterations   (c) 60 iterations   (d) Final Results
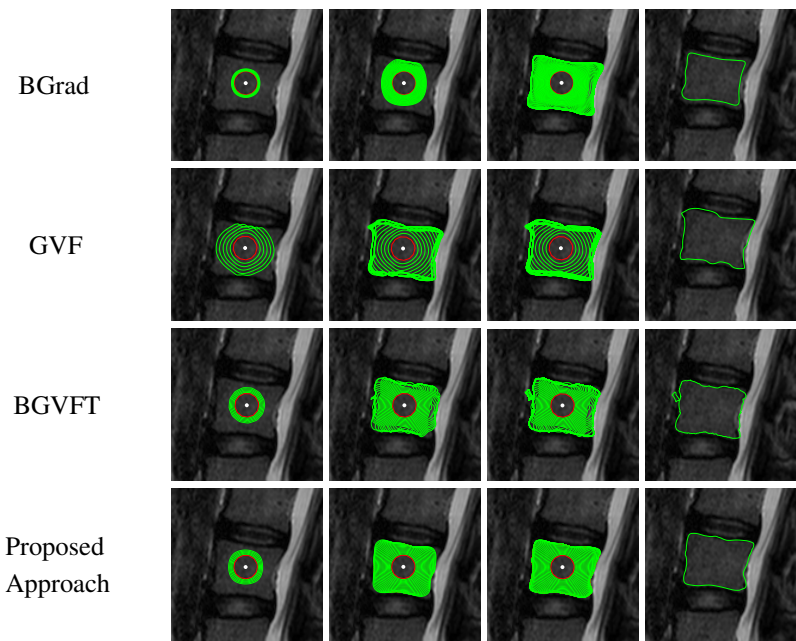
Figure 4: Snake deformation process (green curves) for experiment 2. The white dot represents the manually selected initial position, the red curve represents the initial snake.

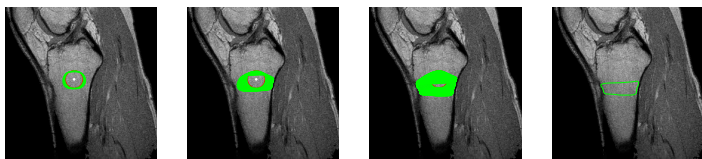(a) 5 iterations   (b) 20 iterations   (c) 60 iterations   (d) Final result

Figure 5: A GVF snake that fails if initialized by a small curve far from the desired boundary.

number of iterations. More iterations may cause snake leakage, unlike our approach which terminates the deformation process when the majority of snake elements encounter strong edges. Visual results for experiment 2 are shown in Fig. 4. The BGrad snake conforms to the desired boundary with high accuracy (DSC=0.8969 ; JC=8130). However, for the same number of iterations required by our proposed approach, this snake does not reach the actual edge. More iterations may cause snake leakage around weak edges if the balloon force is greater than the gradient force. The GVF and BGVFT snakes result in leakages around weak edges. Our approach successfully conforms to the desired boundary with high accuracy.

Note that although the capture range of F_{GVF} is in general large, methods using this external force exclusively may fail if the snake is initialized far from the desired boundary using a relatively small initial curve (see Fig. 5). The GVF field around such small initial snakes may not point towards the desired boundary due to the high levels of noise and clutter. An initial snake closer to the boundary may increase segmentation accuracy in this case.

4   Conclusion

This paper proposed an approach that combines balloon and GVF forces for parametric snakes, and a mechanism to automatically terminate the snake's deformation process. The approach uses a weighting factor to leverage the advantages of these two forces according to

local image features. In smooth areas, balloon forces guide the snake to the object's boundary, while in the presence of strong edge information GVF forces make the snake conform to the boundary. Experimental results on real medical images show that the proposed approach outperforms methods based on traditional external forces, while offering the advantage of initializing the snake with a single manually selected point inside the desired region and terminating the deformation process automatically.

References

[1] Scott T Acton and Nilanjan Ray. Biomedical image analysis: segmentation. *Synthesis Lectures on Image, Video, and Multimedia Processing*, 4(1):1–108, 2009.

[2] Laurent D Cohen. On active contour models and balloons. *CVGIP: Image understanding*, 53(2):211–218, 1991.

[3] Lee R Dice. Measures of the amount of ecologic association between species. *Ecology*, 26(3):297–302, 1945.

[4] Paul Jaccard. The distribution of the flora in the alpine zone. *New phytologist*, 11(2): 37–50, 1912.

[5] Michael Kass, Andrew Witkin, and Demetri Terzopoulos. Snakes: Active contour models. *International Journal of Computer Vision*, 1(4):321–331, 1988.

[6] A. Khadidos, V. Sanchez, and C.-T. Li. Active contours based on weighted gradient vector flow and balloon forces for medical image segmentation. *in Proceedings of International Conference on Image Processing*, Paris, Oct. 27-30, 2014, in press.

[7] Bing Li and Scott T Acton. Active contour external force using vector field convolution for image segmentation. *IEEE Trans. on Image Proc.*, 16(8):2096–2106, 2007.

[8] Liana M Lorigo, Olivier Faugeras, W Eric L Grimson, Renaud Keriven, and Ron Kikinis. Segmentation of bone in clinical knee MRI using texture-based geodesic active contours. In *Medical Image Computing and Computer-Assisted Intervention*, volume 1496, pages 1195–1204. Springer, 1998.

[9] Zhen Ma, João Manuel RS Tavares, Jorge R Natal, and T Mascarenhas. A review of algorithms for medical image segmentation and their applications to the female pelvic cavity. *Comp. Methods in Biomechanics and Biomedical Eng.*, 13(2):235–246, 2010.

[10] S.-E.-A. Raza, V. Sanchez, G. Prince, J. Clarkson, and RajpootN. M. Registration of thermal and visible light images using silhouette extraction. *Pattern Recognition*, in press.

[11] Yuwei Wu, Yuanquan Wang, and Yunde Jia. Adaptive diffusion flow active contours for image segmentation. *Comput. Vis. Image Und.*, 117(10):1421–1435, 2013.

[12] Chenyang Xu and Jerry L Prince. Snakes, shapes, and gradient vector flow. *IEEE Transactions on Image Processing*, 7(3):359–369, 1998.

[13] Yuhua Yao, Lixiong Liu, Lejian Liao, Ming Wei, Jianping Guo, and Yinghui Li. Sigmoid gradient vector flow for medical image segmentation. In *11th International Conference on Signal Processing (ICSP)*, volume 2, pages 881–884. IEEE, 2012.

[14] Huiyu Zhou, Xuelong Li, Gerald Schaefer, M Emre Celebi, and Paul Miller. Mean shift based gradient vector flow for image segmentation. *Computer Vision and Image Understanding*, 117(9):1004–1016, 2013.

[15] Guopu Zhu, Shuqun Zhang, Qingshuang Zeng, and Changhong Wang. Gradient vector flow active contours with prior directional information. *Pattern Recognition Letters*, 31 (9):845–856, 2010.

[16] Christophe Zimmer, Elisabeth Labruyere, Vannary Meas-Yedid, Nancy Guillen, and J-C Olivo-Marin. Segmentation and tracking of migrating cells in videomicroscopy with parametric active contours: A tool for cell-based drug testing. *IEEE Trans. on Medical Imaging*, 21(10):1212–1221, 2002.